Korean J. Chem. Eng., **25**(4), 897-904 (2008)

Effect of pressure fluctuations on the heat transfer characteristics in a pressurized slurry bubble column

Suk-Hwan Kang*, Sung-Mo Son, Yong Kang**,†, Jong-Wook Bae*, and Ki-Won Jun***

*Advanced Chemical Technology Division, Korea Research Institute of Chemical Technology, Daejeon 305-600, Korea
**School of Applied Chemistry and Biological Engineering, Chungnam National University, Daejeon 305-764, Korea
(*Received 21 July 2007 • accepted 16 January 2008*)

Abstract−The hydrodynamics and heat transfer characteristics were investigated in a slurry bubble column reactor whose diameter was 0.0508 m (ID) and 1.5 m in height. Effects of gas velocity (0.025-0.1 m/s), pressure (0.1-0.7 MPa), solid concentration (0-20 vol%) and liquid viscosity (1.0-38.0 mPa s) on the hydrodynamics and heat transfer characteristics were examined. The pressure difference fluctuations were analyzed by means of attractor trajectories and correlation dimension to characterize the hydrodynamic behavior in the column. The gas holdup increased with increasing gas velocity or pressure, but decreased with increasing solid concentration or liquid viscosity. It was found that the attractor trajectories and correlation dimension of pressure fluctuations were effective tools to describe the hydrodynamic behaviors in the slurry bubble column. The heat transfer coefficient increased with increasing pressure or gas velocity, but decreased with increasing solid concentration or viscosity of slurry phase in the slurry bubble column. The heat transfer coefficient value was well correlated in terms of operating variables and correlation dimension of pressure fluctuations in the slurry bubble column.

Key words: Pressurized Bubble Column, Slurry Phase, Heat Transfer Coefficient, Hydrodynamics, Pressure Fluctuations

INTRODUCTION

Slurry bubble column reactors (SBCR) which are operating at high pressure have been widely used for the industrial applications of syngas conversion reactions such as Fischer-Tropsch synthesis and methanol synthesis, heavy oil upgrading, environmental pollution control, and biotechnology. They have several advantages including high heat and mass transfer rates, isothermal conditions, plug-free operation, and on-line catalyst addition and withdrawal [1-4].

However, experiments at laboratory scale to perform Fischer-Tropsch synthesis have been mainly conducted in a slurry tank stirred reactor (STSR) not in an SBCR for lack of information and development on the slurry bubble column reactor. For the commercial design or scale-up of the SBCR, an understanding of the characteristics such as mixing among gases, liquid and particles, gas holdup and heat and mass transfer in the SBCR are essential [5,6]. In addition, the flow behavior and characteristics of gas phase are known to play critical roles in determining the heat transfer coefficient, since the gas bubbles, which exist as a dispersed phase, are flowing stochastically and randomly in the viscous liquid as solvent with particles at high pressure [4,7-9].

In a dynamic flow system such as slurry bubble column reactor, the hydrodynamic stability has to be controlled and adjusted to provide the heterogeneous reactants with plausible conditions for contacting and reaction. However, there has been little attention on the effects of hydrodynamic stability on transport phenomena such as heat and mass transfer and bubbling phenomena in slurry bubble column reactors. The reason why the slurry bubble column reactor has not been developed in spite of its several inherent merits can be partly due to the lack of knowledge on the operational skills related to the system stability, especially at high pressure [3,10].

In the present study, thus, hydrodynamic bubbling behaviors in the slurry bubble column were analyzed by means of the phase space portraits and correlation dimension of the time series of pressure fluctuations. In addition, the heat transfer phenomena were examined with operation variables such as gas velocity, slurry viscosity, pressure and solid concentration in the slurry phase.

ANALYSIS

1. Phase Space Portraits

The highly complicated pressure fluctuations can be visualized more conveniently by means of phase space portraits. The visualization of the data in space phase portraits gives some qualitative information about the physical behavior in the bed. Multidimensional phase space portraits can be constructed from the pressure fluctuation time series by means of the time delay method [11,12]. That is, the experimentally obtained time-series signal, X(t), is digitized with a time step of Δt; the resultant (m+1) values of the signal, X(iΔt), are stored for i=0, 1, 2, ..., m.

Thus, the vector time series is defined as

$$Z_i(t) = [X(i\cdot\Delta t), X(i\cdot\Delta t+\tau), \ldots, X(i\cdot\Delta t+(p-1)\cdot\tau)], \quad i=0, 1, 2, \ldots, [m-(p-1)\cdot k] \tag{1}$$

where $\tau = k\cdot\Delta t$, k=1, 2, 3, …

and p is the dimension of the vector, Z(t). Therefore, moving along with time t, a series of p-dimensional vectors representing the p-dimensional portrait of the system can be obtained. Occasionally, p is referred to as the embedded phase-space dimension of the reconstructed trajectory or attractor.

2. Correlation Dimension

The complexity of the reconstructed attractor is analytically eval-

†To whom correspondence should be addressed.
E-mail: kangyong@cnu.ac.kr

uated with the correlation dimension that is theoretically related to the degree of the freedom of the system. That is, a larger value of correlation dimension means greater complex of the underlying system. Given a scalar time-series signal, X(t), the first step in estimating the correlation dimension (D_C) is to reconstruct the trajectory by resorting to time embedding. The correlation integral (the space correlation function) of the process, C(r), is defined as [13,14]:

$$C(r)=\lim_{m\to\infty}\frac{1}{m^2}\left[\begin{array}{l}\text{number of pairs (i,j) whose distance}\\ |Z_i(t)-Z_j(t)|<r\end{array}\right] \quad (2)$$

Formally,

$$C(r)=\lim_{m\to\infty}\frac{1}{m^2}\sum_{i=1}^{m}\sum_{j=1}^{m}H[r-|Z_i(t)-Z_j(t)|], \quad i\neq j \quad (3)$$

where m is the number of data points, and H is Heaviside function,

$$H[r-|Z_i(t)-Z_j(t)|]=\begin{cases}1 \text{ if } r>|Z_i(t)-Z_j(t)|\\ 0 \text{ otherwise}\end{cases} \quad (4)$$

The correlation integral, C(r), has been found to be a power function of r for small r's:

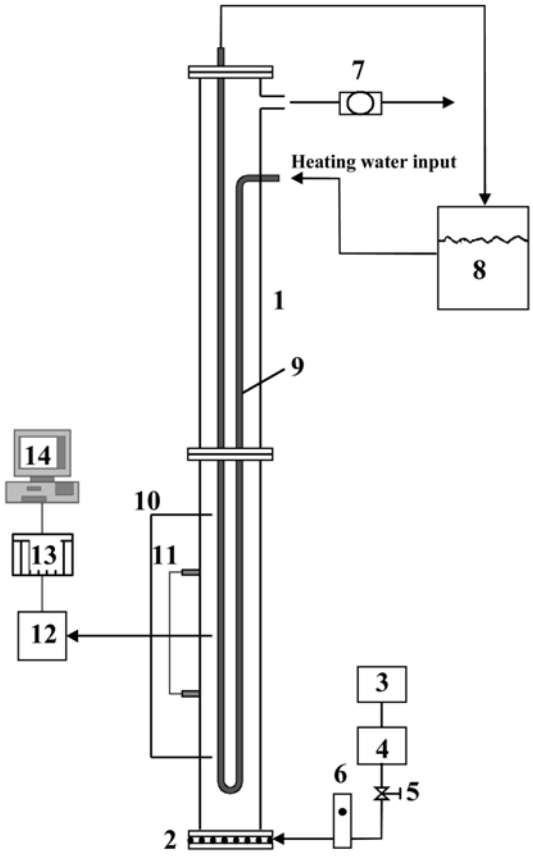

Fig. 1. Experimental apparatus.

1. Main column
2. Distributor
3. Compressor
4. Filter and regulator
5. Valve
6. Flowmeter
7. Back pressure regulator
8. Thermostat
9. Heating tube
10. Thermocouples
11. Pressure sensor
12. Low-pass filter
13. A/D convertor
14. Computer

$$C(r)=kr^{Dc} \quad (5)$$

The exponent, D_C, is defined as the correlation dimension as

$$\ln C(r)=D\ln r+\ln k \quad (6)$$

The slope of the plot of lnC(r) vs lnr is an estimate of D_C for the given embedded space dimension, p.

EXPERIMENTS

Experiments were performed in a stainless steel column of 0.0508 m in diameter and 1.5 m in height as shown in Fig. 1. Oil-free compressed air was fed to the column through a pressure regulator, filter and a calibrated flow meter. It was admitted to the column through three 3.0 mm ID perforated pipes drilled horizontally in the grid. The pipes were evenly spaced across the grid having 12 holes whose diameter is 1 mm.

The dynamic pressure fluctuations were measured at the center of the bed through the pressure taps that were mounted flush with the wall of the column between 0.1 and 0.2 m from the distributor. Pressure fluctuations were measured and detected by sensitive differential pressure transducer (Validyne, Model P24D) attached to the pressure probes. The voltage-time signals, corresponding to the pressure-time signals, were sampled at a rate of 300/s and stored in the data acquisition system (Data Precision-Model, DT2805). The total acquisition time was 10 s having 3000 data points.

The superficial gas velocity was in the range of 0.05-0.1 m/s. Aqueous solutions of CMC (carboxymethylcellulose) were used as liquid phase to make the slurry phase. Silica gel powder whose diameter was in the range of 0.063-0.2 mm was used to comprise the slurry phase. The concentration of solid in the slurry phase was in the range of 0-20 vol%. The operating pressure in the column was in the range of 0.1-0.7 MPa.

The individual heat transfer coefficient between the fluidizing medium and the surface of heat transfer tube was determined. The

Table 1. Composition of the concentrated synthetic wastewater

Concentration (g/L)	Component
5.6	Glucose
9.7	$CH_3COONa\cdot 3H_2O$
1.32	KH_2PO_4
0.006	$FeCl_3\cdot 6H_2O$
0.075	$CaCl_2$
2.8	$(NH_4)_2SO_4$
1.0	$MgSO_4\cdot 7H_2O$
0.1098	$MnSO_4\cdot H_2O$
2.1	$NaHCO_3$

Table 2. Liquid physical properties and fluids flow rate range

Solution	ρ_L kg/m^3	$\mu_L\times 10^3$ Pa·s	n	$\sigma_L\times 10^3$ N/m	$U_G\times 10^2$ m/s
Water	1,000	0.96	1.000	72.9	1.0-7.0
CMC(1)	1,001	11	0.882	73.2	1.0-7.0
CMC(2)	1,002	24	0.847	73.3	1.0-7.0
CMC(3)	1,003	38	0.825	73.6	1.0-7.0

relation between the overall (U) and the individual heat transfer coefficients (h_o) could be expressed as;

$$\frac{1}{U}=\frac{1}{h_o}+\frac{x_t}{k_t}\frac{A_o}{A_L}+\frac{A_o}{A_i}\frac{1}{h_i} \tag{7}$$

where A_i and A_o were internal and external areas of heat transfer tube. The logarithmic mean area of heat transfer tube was defined as $(A_o-A_i)/\ln(A_o/A_i)$, k_t was thermal conductivity of heat transfer tube, and x_t was thickness of heat transfer tube, respectively.

Heat transferred from the slurry bubble column to water in the immersed heat transfer tube (Q_1), and the recovered heat by water in the immersed heat transfer tube (Q_2) could be expressed as:

$$Q_1=UA_o\Delta T_{lm} \tag{8}$$

$$Q_2=m_wC_{pw}(T_{wo}-T_{wi}) \tag{9}$$

where m_w is water flow rate in the heat transfer tube, C_{pw} specific heat of water, and ΔT_{lm} logarithmic mean temperature difference between the bed and water in the immersed tube defined as $(T_{wo}-T_{wi})/\ln[(T_b-T_{wi})/(T_b-T_{wo})]$, respectively.

Thus, the overall heat transfer coefficient in the slurry bubble column was obtained from Eqs. (8) and (9) as:

$$U=m_wC_{pw}(T_{wo}-T_{wi})/A_o\Delta T_{lm} \tag{10}$$

In Eq. (7), the inside individual heat transfer coefficient (h_i) between the fluid and the internal surface of the heat transfer tube was given by Bennett and Myers (1974);

$$h_i=1.75\left(\frac{k_w}{D_i}\right)\left(\frac{m_w}{k_w}\frac{C_{pw}}{L}\right)^{1/3} \tag{11}$$

where D_i is inner diameter of heat transfer tube, k_w thermal conductivity of water and L length of heat transfer tube. Therefore, the heat transfer coefficient (h_o) was determined from Eqs. (7), (10) and (11).

The heat transfer tube made of copper was located vertically as U type in the slurry bubble column [15]. The heat capacity and conductivity of this tube were 386 J/kg K and 383 W/m K, respectively. The tube was 0.8 m long with an inside diameter of 0.92 cm and an outside diameter of 1.37 cm. As a heat source, hot water heated in a 10 *l* surge tank by immersion heater was circulated with a velocity of 0.3 *l*/min through the tube at close to 333 K.

RESULTS AND DISCUSSION

Typical examples of effects of operating variables such as gas velocity, solid concentration, slurry viscosity and pressure on the gas holdup in a slurry bubble column can be seen in Fig. 2. In Fig. 2(a), the gas holdup increases with increasing gas velocity in all the cases studied. In a bubble column without solid, the dependence of gas holdup on the gas velocity has been generally in the form of $\varepsilon_G \propto U_G^n$. The value of n depends on the flow regime; in the bubbly flow regime, the value of n varies from 0.7 to 1.2; while in the churn turbulent or the transition regime, the effect of gas velocity has been less pronounced and the exponent *n* takes values from 0.4 to 0.7 [1]. Therefore, it is plausible that the operating condition of this study belongs to the bubbly flow regime, since the n value was in the range of 0.7-1.2.

As it can be seen in Fig. 2(b), the gas holdup decreases gradually with increasing the solid concentration in the slurry phase and the slurry viscosity in the column. This behavior is related to the fact that the increase of solid concentration can lead to the increase of slurry viscosity which promotes the formation of larger gas bubbles. Furthermore, if the pressure and gas velocity are maintained at constant level, the gas momentum per unit mass of slurry would decrease with increasing solid concentration and thus, the total gas holdup is expected to decrease with increasing solid amount [7]. The slurry viscosity seems to have a strong impact on the gas holdup [3,7]. In Fig. 2(b), the value of gas holdup tends to decrease gradually with increasing liquid viscosity. This can be because the interfacial tension of bubbles increases and the boundary layer thickness of the bubbles becomes to be thick; thus, bubble size increases with increasing liquid viscosity. That is, the gas holdup decreases by the increase of bubble size and rising velocity since the turbulent intensity of the liquid, which can pulverize the bubbles, would decrease with increasing slurry viscosity.

Effects of pressure on the gas holdup in the slurry bubble column can be seen in Fig. 2(c). As it can be seen, the gas holdup increases

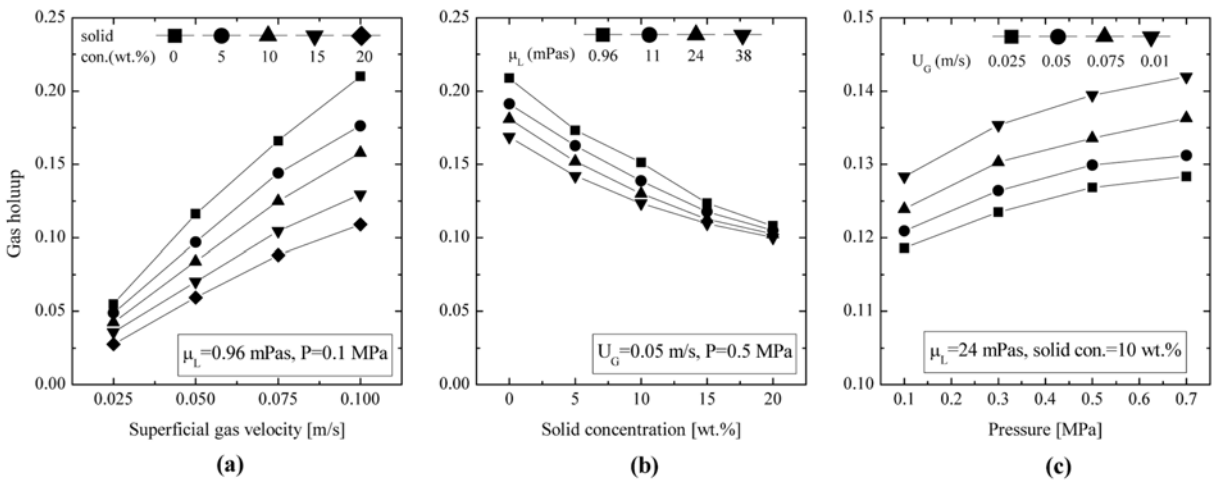

Fig. 2. Effects of gas velocity, solid concentration and pressure on the gas holdup in slurry bubble columns.

with increasing pressure. The values of gas holdup are associated with the rising velocity and number density of bubbles in the column. The pressure affects the hydrodynamics in the column through the variation in bubble size and its distribution. The increase of gas holdup with pressure is mainly due to the increase of small gas bubbles [16]. In addition, the distribution of bubble size is narrow and the size and intensity of wakes decrease with decreasing bubble size, trapping fewer trailing bubbles; the difference in bubble velocities decreases by being increased size uniformity; and non-uniformity of the local flow field decreases since bubble size and wake intensity have been decreased [17].

Typical examples of pressure fluctuations in slurry bubble columns can be seen in Fig. 3. In this figure, the amplitude of differential pressure (ΔP) fluctuation signals increases with increasing gas velocity. The signals become more complex with increasing U_G.

Those pressure fluctuations can be utilized more conveniently to visualize the complex flow behavior of multiphase in the slurry bubble column by means of phase space portraits in the reconstructed trajectory. The optimum time lag, τ, for the construction of attractors in the phase space has been chosen as 0.003 s corresponding to the first minimum value in the mutual information function [10].

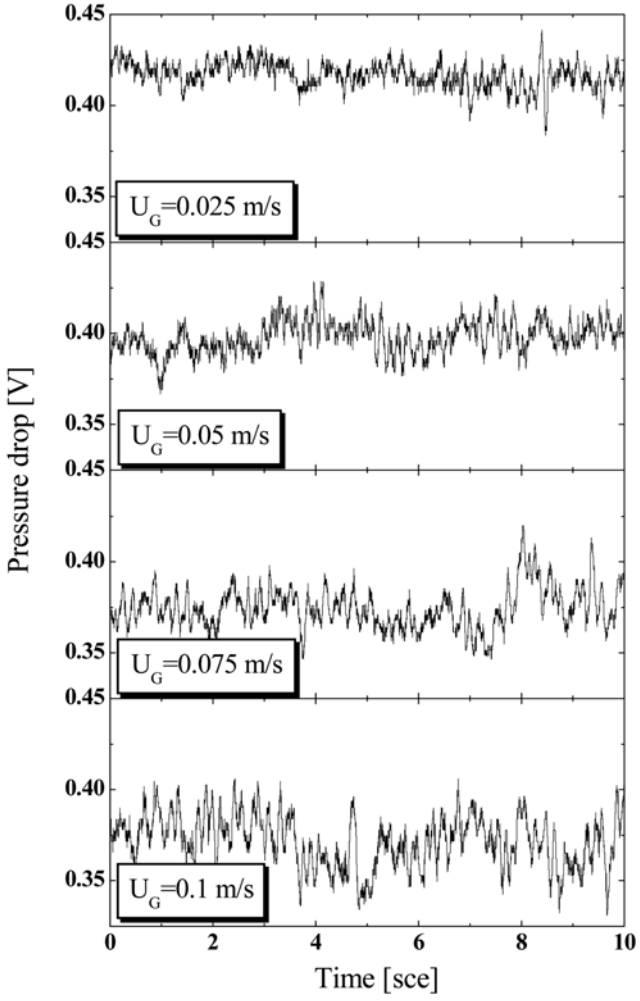

Fig. 3. Typical examples of pressure fluctuations in the slurry bubble columns (μ_L=24 mPas, P=0.5 MPa, solid con.=15 wt.%).

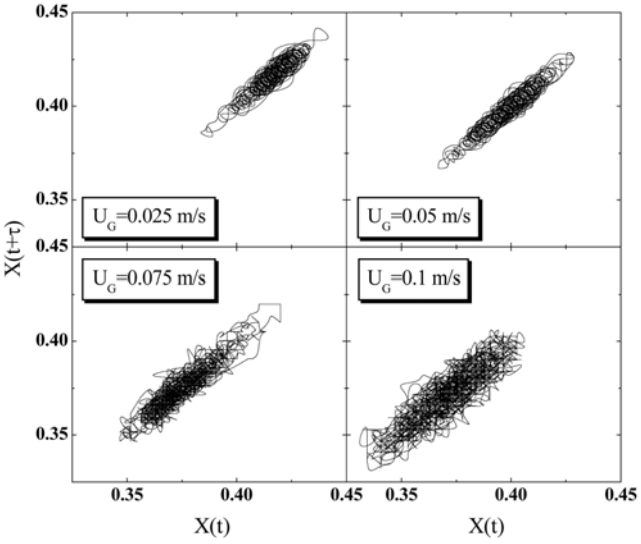

Fig. 4. Typical examples of phase space portraits of pressure fluctuations in the slurry bubble columns (μ_L=24 mPas, P=0.5 MPa, solid con.=15 wt.%).

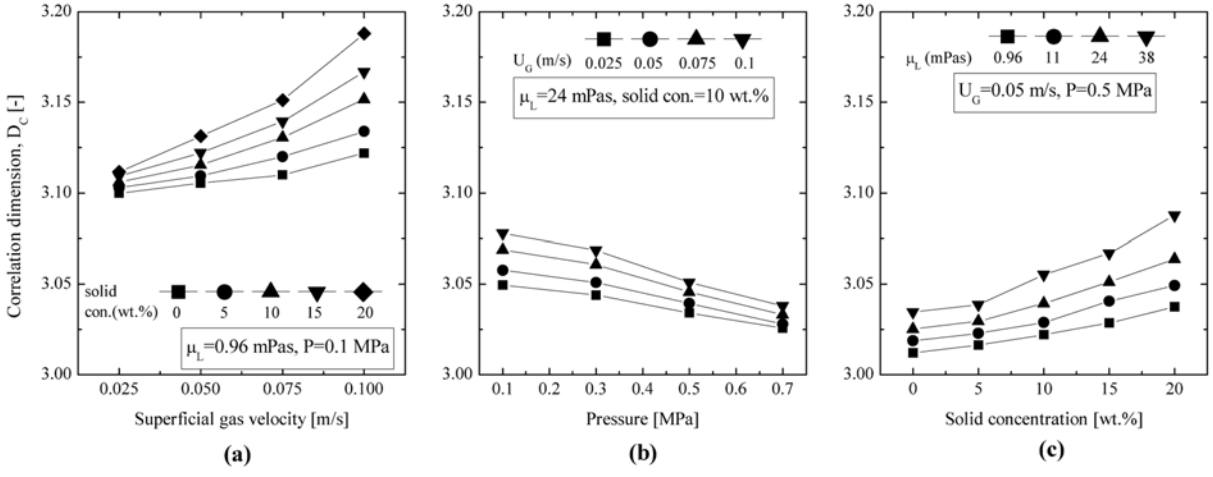

Fig. 5. Effects of gas velocity, pressure, solid concentration and slurry viscosity on the correlation dimension in slurry bubble column.

The examples of phase space portraits of pressure fluctuation data can be seen in Fig. 4, with the variations of U_G. It can be noted in this figure that the attractor becomes more scattered and complicated with increasing U_G. To elucidate the dynamic characteristics of hydrodynamic phenomena in the slurry column more easily and quantitatively, the correlation dimension, D_C, of the pressure fluctuations was calculated [13].

Effects of gas velocity on the correlation dimension of pressure fluctuations can be seen in Fig. 5(a). In this figure, the D_C value increases with increasing gas velocity but decreases with increasing pressure (Fig. 5(b)). Since the correlation dimension is a measure of the spatial homogeneity in the phase space, the increment of D_C means that the underlying system becomes non-homogeneous and more complicated and chaotic [18-20]. It is anticipated from these that the predictability of hydrodynamic phenomena diminishes in the slurry bubble column with increasing U_G, owing to a great deal of complex information. On the other hand, it can be stated that the dynamic phenomena in the bubble column become more homogeneous and regular with increasing pressure, while they become more complex and irregular with increasing U_G.

Effects of solid concentration and slurry viscosity on the correlation dimension of pressure fluctuations can be seen in Fig. 5(c). In this figure, the values of D_C increase with increasing solid concentration or liquid viscosity. These can be due to the increase of solid amount in the column. It is noted that the bubble size increases gradually with increasing liquid viscosity in the column. The distribution of bubble size becomes wide with increasing the bubble size in the column; thus, the predictability of the dynamic behavior would decrease with increasing solid concentration or slurry viscosity. To analyze the bubbling behavior in the slurry bubble column, the interstitial gas velocity can be utilized based on the drift flux model [21-23]. That is, the non-uniform of bubble holdup can be detected in the churn turbulent flow regime by Eq. (12).

$$\frac{U_G}{\varepsilon_G} = KU_G + U_O \tag{12}$$

In Eq. (12), K is a constant related to the degree of non-uniform in the bubble column, and U_O is the value corresponding to the rising velocity of a single bubble in the bubble column. As can be seen in Fig. 6, the results of this study are well fitted to Eq. (12), since the plots are essentially linear in any case. Note that the values of K and U_O decrease with increasing the pressure. This implies that the degree of uniformity of bubbling phenomena increases and bubble rising velocity decreases, with increasing pressure.

The heat transfer coefficient (h_o) was determined by means of Eqs. (7)-(11) from a knowledge of the mean value of differential temperature between the immersed heat transfer tube and the bed. Effects of gas velocity on the heat transfer coefficient can be seen in Fig. 7. In this figure, the h values increase with increasing U_G in all cases. This can be attributed to the increase of turbulence in the

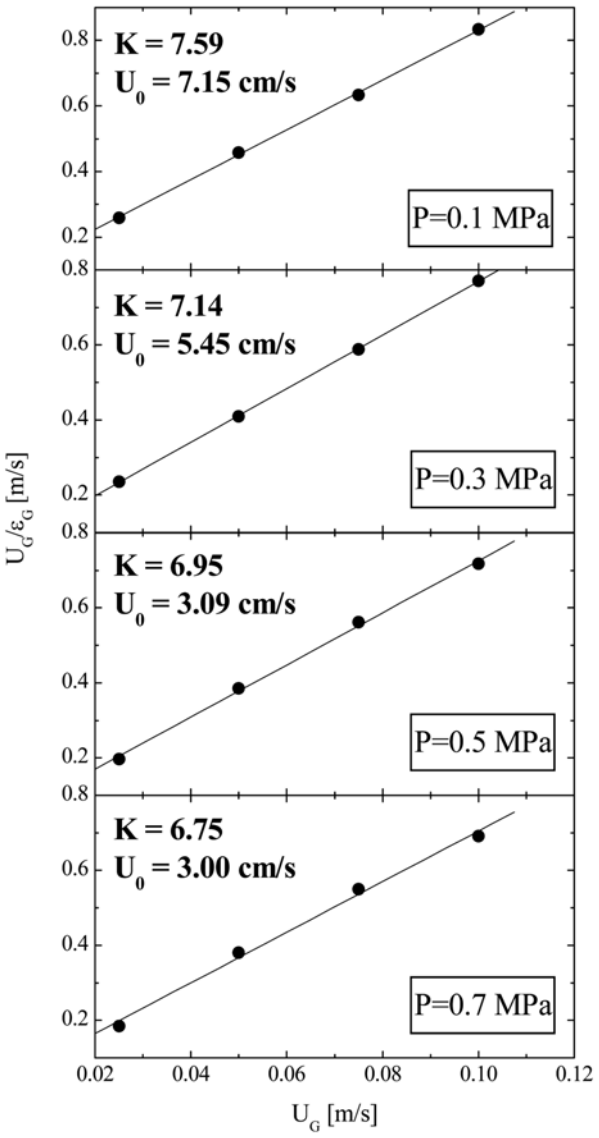

Fig. 6. Typical examples of gas velocity plots based on the drift flux theory in the slurry bubble columns (μ_L=24 mPas, solid con. =10 wt.%).

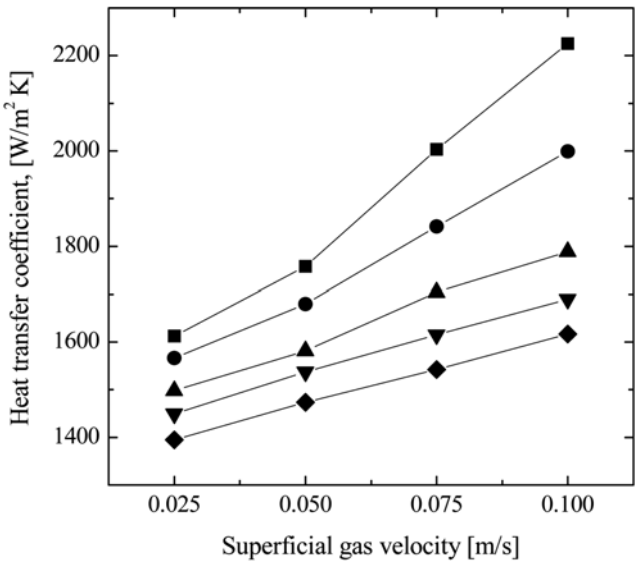

Fig. 7. Effects of gas velocity on the heat transfer coefficient in slurry bubble columns (μ_L=0.96 mPas, P=0.1 MPa).

Solid con. (wt.%) 0 5 10 15 20

slurry bubble column due to the increases of gas holdup and gas momentum flow rate with increasing U_G [8,24]. As a result, the increase of turbulent intensity, with making the boundary layer thickness at the surface area of heat transfer tube to be thin, would take out the high h values.

Effects of pressure on the heat transfer coefficient can be seen in Fig. 8. In this figure, the heat transfer coefficient increases with increasing pressure. It has been understood that the bubble size decreases with an increase in the pressure, which results in the increase of gas holdup and thus increase of the periodic turbulence by means of bubble passage in the column. These consequently result in the increase of heat transfer coefficient in the column.

Effects of the solid concentration on the heat transfer coefficient can be seen in Fig. 9. In this figure, the value of heat transfer coefficient decreases slowly with increasing solid concentration and slurry viscosity. This can be attributed to an increase in apparent slurry viscosity and corresponding increase in average boundary layer thickness at the tube surface for heat transfer, with increasing slurry concentration [9,25]. The value of the heat transfer coefficient decreases gradually with increasing liquid viscosity, since the bubble size in-

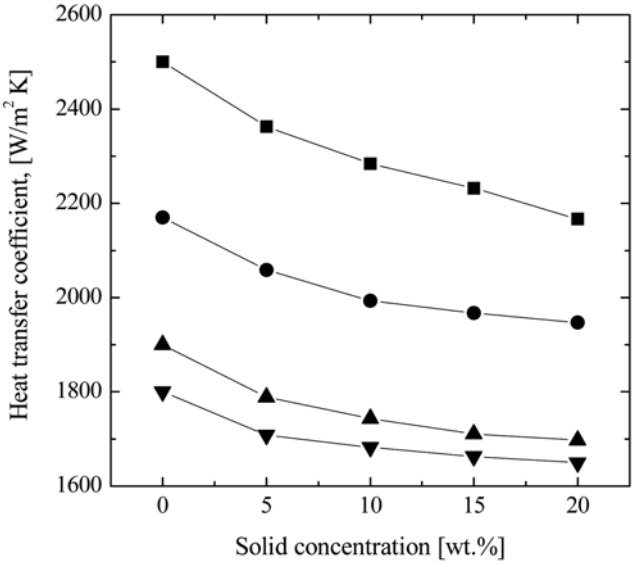

Fig. 8. Effects of solid concentration and slurry viscosity on the heat transfer coefficient in slurry bubble columns (U_G=0.05 m/s, P=0.3 MPa).

	-■-	-●-	-▲-	-▼-
μ_L (mPas)	0.96	11	24	38

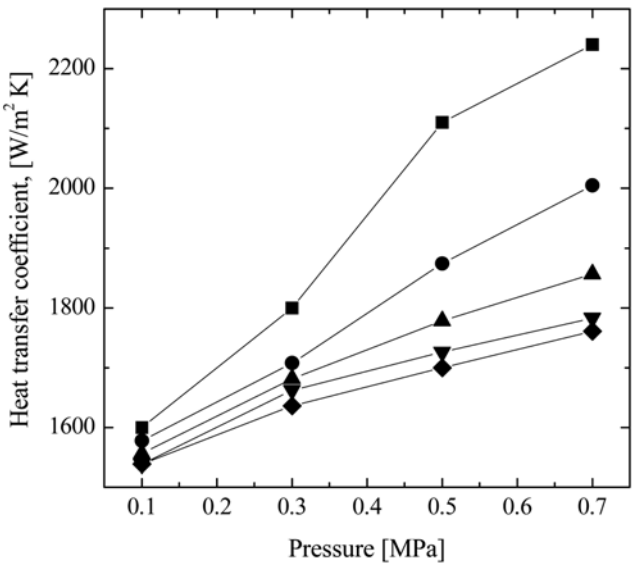

Fig. 9. Effects of pressure on the heat transfer coefficient in slurry bubble columns (μ_L=38 mPas, U_G=0.05 m/s).

	-■-	-●-	-▲-	-▼-	-◆-
solid con. (wt.%)	0	5	10	15	20

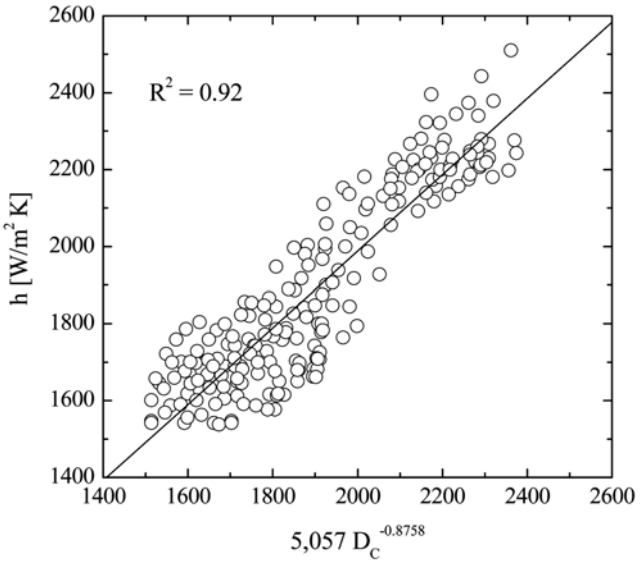

Fig. 10. Relation between the heat transfer coefficient and the correlation dimension of pressure fluctuations in slurry bubble columns.

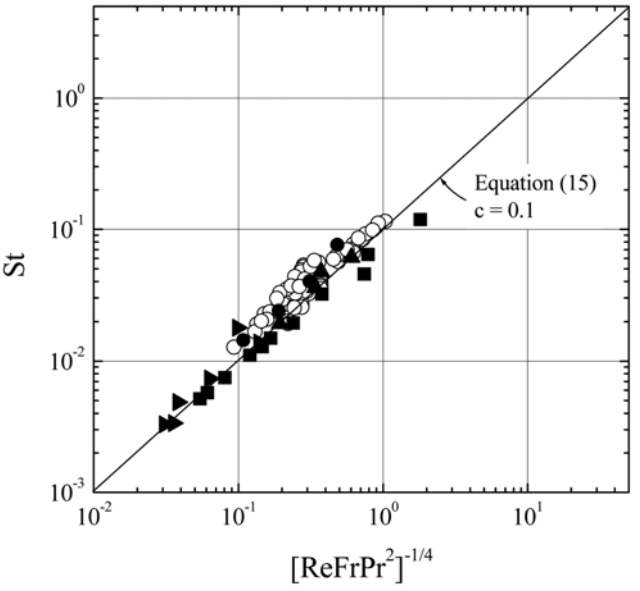

Fig. 11. Correlation of heat transfer coefficient measured in slurry phase based on Eq. (15) (material systems and symbols given in Table 3).

Table 3. Slurry systems used to check the validity of Eq. (15); see Fig. 11

Author	Solid phase	Solid content (wt%)	Temperature (°C)	Viscosity (mPa s)	Symbol in Fig. 11
Müller [26]	Water-kieselguhr	18.0	20-26	99	■
Martins [27]	Water-sand				
	40 μm	20.0	25	1.4	●
Deckwer et al. [28]	Paraffin-Al_2O_3	5.5-16.0	220	4.3-4.8	▲
		5.5-16.0	260	2.1-2.3	▶
This work	CMC Sol'n-silica gel	0-20	25	0.96-38	○

creases with increasing liquid viscosity. In other words, the residence time of bubbles in the column decreases owing to the increase of rising velocity of bubbles. This reduces bubble holdup considerably in the column. Moreover, the size distribution of bubbles becomes wider with increasing the bubble size, which can lead to the generation of the more irregular bubbling phenomena, as depicted in the space portraits and correlation dimension of pressure fluctuations.

$$h_o = 2{,}547 U_G^{0.0198} P^{0.1047} S_C^{-0.0109} \mu_L^{-0.0485} \quad (13)$$

The value of the heat transfer coefficient was well correlated in terms of operating variable as Eq. (13) with a correlation coefficient of 0.93. Since the heat transfer coefficient is closely related to the bubbling phenomena in the slurry bubble column, the value of h_o was also correlated with the correlation dimension of pressure fluctuations in the column as Eq. (14). As it can be seen in Fig. 10, Eq. (14) was well fitted with the experimentally obtained heat transfer coefficient with a correlation coefficient of 0.92.

$$h_o = 5{,}0.57 D_C^{-0.8758} \quad (14)$$

However, Eq. (13) correlated in terms of operating variable can be written dimensionless,

$$St = C(ReFrPr2)^{-1/4} \quad (15)$$

Fig. 11 represents the Stanton number plotted against the dimensionless group $(ReFrPr^2)^{-1/4}$ for various slurry systems in Table 3. As expected, Eq. (15) fits just as well as it does the reference's data [26-28] and our data, producing a figure of C=1 for heat transfer.

CONCLUSION

Hydrodynamics and heat transfer characteristics were successfully analyzed and discussed in pressurized slurry bubble columns, by means of chaos analysis of pressure fluctuations and determination of heat transfer coefficient. It was found that the attractor trajectories and correlation dimension of pressure fluctuations could be effective tools to describe and analyze the complex hydrodynamic behaviors of pressurized slurry bubble column. The gas holdup in pressurized slurry bubble columns increased with increasing gas velocity or pressure, but decreased with increasing solid concentration or slurry viscosity. The heat transfer coefficient in the column increased with increasing gas velocity or pressure, but decreased with increasing solid concentration or viscosity of slurry phase. The value of the heat transfer coefficient was well correlated in terms of operating variables and correlations dimension of pressure fluctuations in the pressurized slurry bubble columns.

NOMENCLATURE

A : surface area [m^2]
A_i : tube inside area [m^2]
A_L : equivalent area [m^2]
A_o : tube outside area [m^2]
C_P : heat capacity [J/kg K]
C_{pw} : specific heat of water [J/kg K]
$C(r)$: correlation integral
D_C : correlation dimension
D_i : inside diameter of heat transfer tube [m]
H : heaviside function defined as Eq. (4)
h_i : inside individual heat transfer coefficient [W/m^2 K]
h_o : individual heat transfer coefficient [W/m^2 K]
K : degree of non-uniformity in the radial direction
k_t : thermal conductivity of heat transfer tube [W/m K]
k_w : thermal conductivity of water [W/m K]
L : length of heat transfer tube [m]
m : number of data point
m_w : flow rate of water [kg/hr]
P : pressure [MPa]
p : embedded phase-space dimension
Q : heat flow [W]
Q_1 : heat flow transferred from the slurry bubble column to water in the immersed heat transfer tube [W]
Q_2 : heat flow recovered by water in the immersed heat transfer tube [W]
r : radius of hypersphere
S_C : solid concentration [wt%]
T_b : bed temperature [K]
T_m : logarithmic mean temperature difference [K]
T_{wi} : input temperature in the heat transfer tube [K]
T_{wo} : output temperature in the heat transfer tube [K]
U : overall heat transfer coefficient [W/m^2 K]
U_G : gas velocity [m/s]
$X(t)$: time series of temperature difference fluctuations [K]
x_t : thickness of heat transfer tube [m]
Z_i : the vector time series

Greek Letters

τ : time delay [s]
μ : viscosity [Pa·s]
ρ : density [kg/m^3]

REFERENCES

1. Y. T. Shah, B. G. Kelkar, S. P. Godbole and W.-D. Deckwer, *AIChE J.*, **28**, 353 (1982).
2. L.-S. Fan, *Gas-liquid-solid fluidization engineering*, Butterworth Pub-

lishers, Stoneham, MA, USA (1989).
3. R. Krishna and S. T. Sie, *Fuel Processing Technol*., **64**, 73 (2000).
4. K. Zhang, H. S. Song and D. K. Sun, *Fuel*, **82**, 233 (2003).
5. W.-D. Deckwer, *Bubble column reactors*, John Wiley and Sons, New York. (1992).
6. K. S. Shin, P. S. Song, C. G. Lee, S. H. Kang, Y. Kang and S. D. Kim, *AIChE J*., **51**, 671 (2005).
7. J. R. Inga and B. I. Morsi, *Ind. Eng. Chem. Res*., **38**, 928 (1999).
8. G. Q. Yang, X. Luo, R. Lau and L. S. Fan, *Ind. Eng. Chem. Res*., **39**, 2568 (2000).
9. H. Li, A. Prakash, A. Margaritis and M. A. Bergougnou, *Powder Technol*., **133**, 171 (2003).
10. Y. Kang, Y. J. Cho, K. J. Woo, K. I. Kim and S. D. Kim, *Chem. Eng. Sci*., **55**, 411 (2000).
11. N. H. Packard, J. P. Crutchfield, J. D. Farmer and R. S. Shaw, *Phys. Rev. Lett*., **45**, 712 (1980).
12. J. C. Roux, *Physica D*, **8**, 257 (1983).
13. P. Grassberger and I. Procaccia, *Physica D*, **9**, 189 (1983).
14. N. B. Abraham, A. M. Albano, B. Das, G. De Guzman, S. Yong, R. S. Gioggia, G. P. Puccioni and J. R. Tredicce, *Phys. Lett*., **114A**, 217 (1986).
15. Y. S. Park and J. E. Son, *HWAHAK KONGHAK*, **31**, 287 (1993).
16. U. Jordan, A. K. Saxena and A. Schumpe, *Can. J. Chem. Eng*., **81**, 491 (2003).
17. P. M. Wilkinson and L. L. van Dierendonck, *Chem. Eng. Sci*., **45**, 2309 (1990).
18. K. J. Woo, Y. J. Cho, K. I. Kim, Y. Kang and S. D. Kim, *J. KIChE*, **36**, 937 (1998).
19. Y. Kang, Y. J. Cho, K. J. Woo and S. D. Kim, *Chem. Eng. Sci*., **54**, 4887 (1999).
20. S. M. Son, P. S. Song, C. G. Lee, S. H. Kang, Y. Kang and K. Kusakabe, *J. Chem. Eng. Japan*, **37**, 990 (2004).
21. M. Zuber and J. A. Findly, *J. Heat Transfer*, **87**, 453 (1965).
22. N. N. Clark and R. L. Flemmer, *AIChE J*., **31**, 500 (1985).
23. Y. Kang, J. S. Shin, S. H. Cho, M. J. Choi and K. W. Lee, *J. Chem. Technology Biotechnol*., **63**, 313 (1995).
24. T. J. Lin and L. S. Fan, *Chem. Eng. Sci*., **54**, 4853 (1999).
25. S. K. Kumar and L. S. Fan, *AIChE J.*, **40**, 745 (1994).
26. K. Müller, Dissertation, TU Berlin (1958).
27. J. Martins, Dissertation, TU Berlin (1959).
28. W.-D. Deckwer, Y. Louisi, A. Zaida and M. Ralek, *Ind. Eng. Chem. Proc. Des. Dev.*, **19**, 198 (1980).